Supporting Information

Bimetallic sulfide/N-doped carbon composites derived from Prussian blue analogues/cellulose nanofibers (PBA/CNFs) film toward enhanced oxygen evolution reaction

Zhengping Li [a,*], Feiyang Chen [a], Chunlong Li [a], Zhiliang Zhang [a], Fangong Kong [a], Xipeng Pu [b] and Qifang Lu[c]

[a] State Key Laboratory of Biobased Material and Green Papermaking, Qilu University of Technology (Shandong Academy of Sciences), Jinan, 250353, People's Republic of China

[b] School of Materials Science and Engineering, Shandong Provincial Key Laboratory of Chemical Energy Storage and Novel Cell Technology, Liaocheng University, Liaocheng 252000, People's Republic of China

[c] Key Laboratory of Processing and Testing Technology of Glass and Functional Ceramics of Shandong Province, School of Material Science and Engineering, Qilu University of Technology (Shandong Academy of Sciences), Jinan 250353, People's Republic of China

* Email: knje@163.com

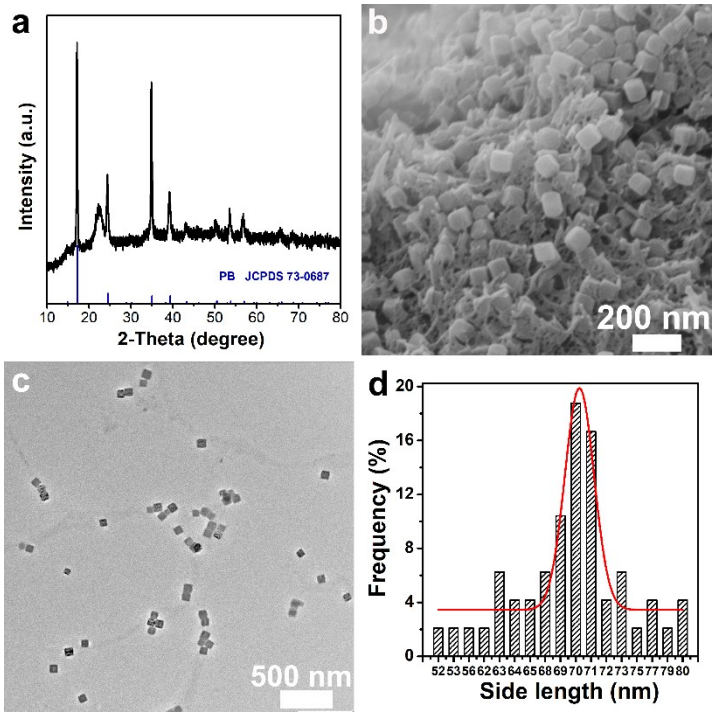

Fig. S1. a) XRD result, b) SEM and c) TEM image of NiFe-PBA/CNFs film, d) histograms of size distribution of NiFe-PBA NPs in NiFe-PBA/CNFs film.

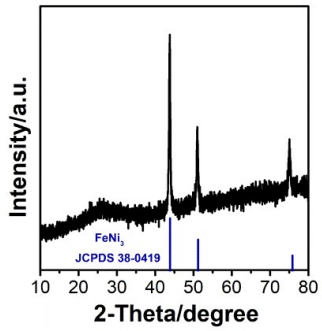

Fig. S2. XRD result of NiFe-alloy/NC composite.

Table S1 Elemental composition of Ni and Fe determined by ICP-OES

Samples	Ni content (mg/L)	Fe content (mg/L)	Ni/Fe molar ratio
$Fe_{0.4}Ni_{0.6}S_2$/NC-DF	9.069	6.092	1.416
$Fe_{0.4}Ni_{0.6}S_2$/ NC-DA	13.90	9.009	1.468
$Fe_{0.4}Ni_{0.6}S$/NC NPs	22.72	15.36	1.407

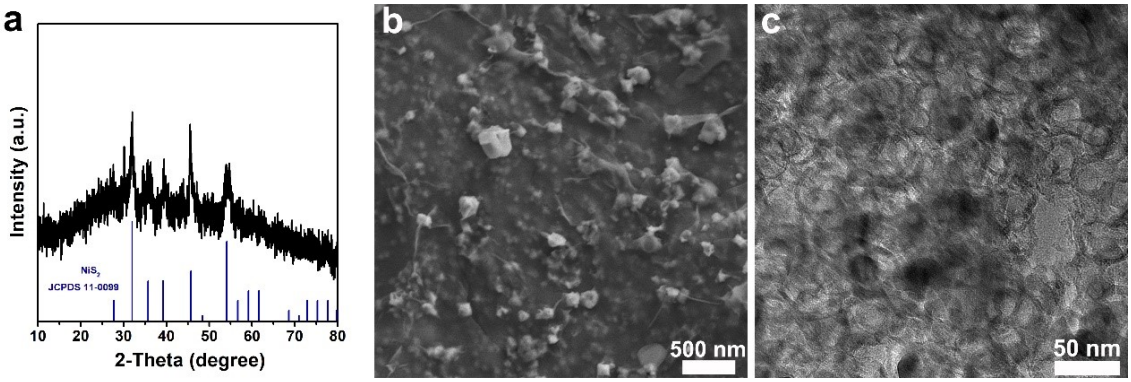

Fig. S3. a) XRD result, b) SEM and c) TEM image of $Fe_{0.4}Ni_{0.6}S_2$/NC-DA.

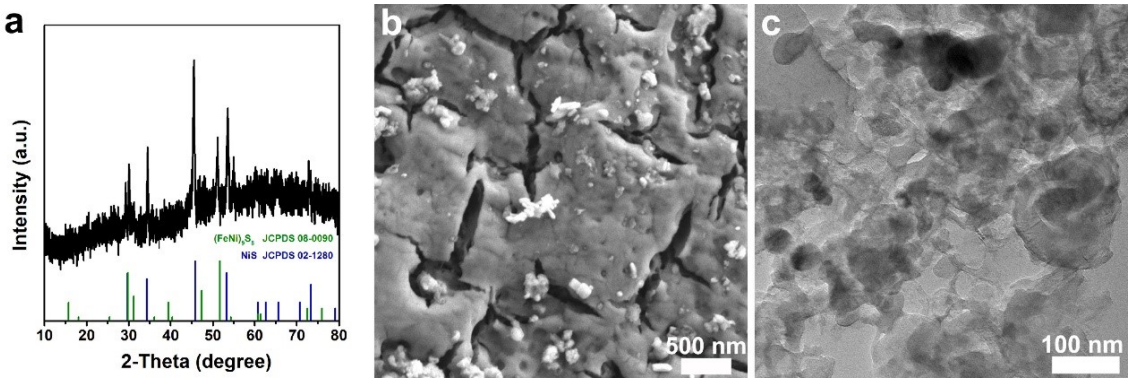

Fig. S4. a) XRD result, b) SEM and c) TEM image of $Fe_{0.4}Ni_{0.6}S$/NC NPs.

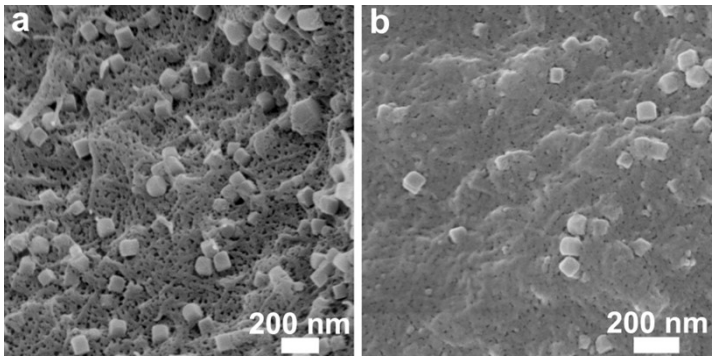

Fig. S5. SEM image of a) NiFe-PBA/CNFs film and b) NiFe-PBA/CNFs aggregates.

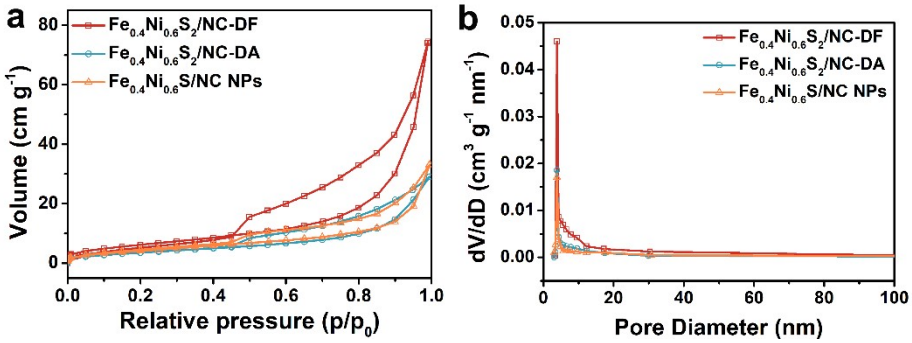

Fig. S6. a) N_2 adsorption–desorption isotherm and b) the pore size distribution curve of $Fe_{0.4}Ni_{0.6}S_2$/NC-DF, $Fe_{0.4}Ni_{0.6}S_2$/NC-DA and $Fe_{0.4}Ni_{0.6}S$/NC NPs.

Table S2 Calculated values of OER electrocatalysts based on the fitted equivalent circuit in 1M KOH.

Samples	R_s (Ω)	R_{ct} (Ω)
$Fe_{0.4}Ni_{0.6}S_2$/NC-DF	9.68	18.62
$Fe_{0.4}Ni_{0.6}S_2$/NC-DA	3.27	271.4
$Fe_{0.4}Ni_{0.6}S$/NC NPs	7.33	63.86
RuO_2	11.78	42.93

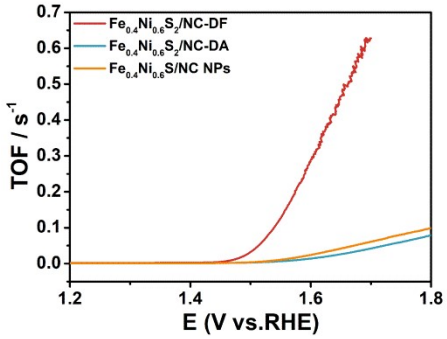

Fig. S7. TOF values of $Fe_{0.4}Ni_{0.6}S_2$/NC-DF, $Fe_{0.4}Ni_{0.6}S_2$/NC-DA and $Fe_{0.4}Ni_{0.6}S$/NC NPs at different potentials.

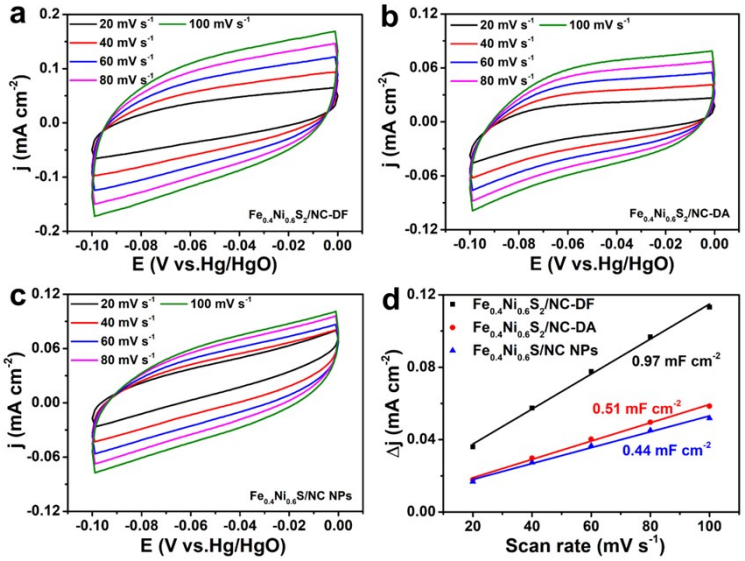

Fig. S8. CV curves of a) $Fe_{0.4}Ni_{0.6}S_2$/NC-DF, b) $Fe_{0.4}Ni_{0.6}S_2$/NC-DA, and c) $Fe_{0.4}Ni_{0.6}S$/NC NPs in the potential range of -0.1-0 V (vs. Hg/HgO) at scanning rate of 20, 40, 60, 80, and 100 mV s^{-1}, and d) linear fitting curve of Δj=1/2(ja-jc) at different scanning speeds at -0.05 V (vs. Hg/HgO)

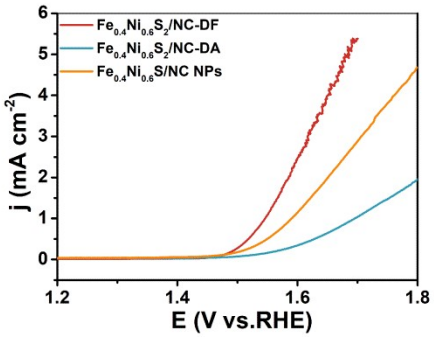

Fig. S9. The specific activity of $Fe_{0.4}Ni_{0.6}S_2$/NC-DF, $Fe_{0.4}Ni_{0.6}S_2$/NC-DA and $Fe_{0.4}Ni_{0.6}S$/NC NPs normalized by ECSA.

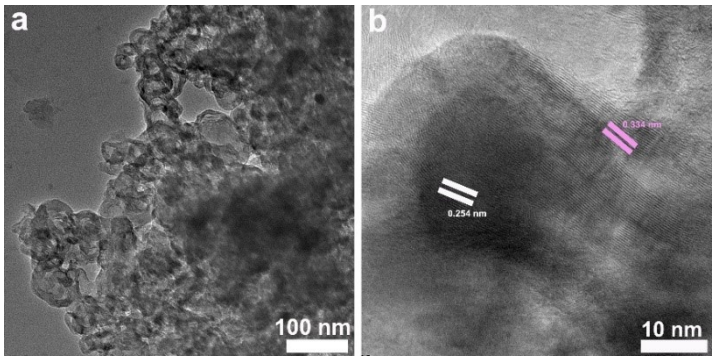

Fig. S10 a) TEM and b) HRTEM image of $Fe_{0.4}Ni_{0.6}S_2$/NC-DF after stability.

Table S3 Comparison of OER performances over nickle sulfide-based electrocatalysts in 1M KOH electrolyte recently reported in the literatures. (η_{OER} are the overpotentials of OER at specific current density)

Catalysts	η_{OER} (mV)	Tafel (mV dec^{-1})	Mass loading (mg cm^{-2})	Substrate	Ref.
$Fe_{0.4}Ni_{0.6}S_2$/NC-DF	**282(10)**	**59.7**	**0.2**	**GC**	**This work**
Fe-NiS_2/MoS_2	280(10)	91.2	0.25	GC	1
Fe-NiS	270(10)	45.3	0.40	GC	2
NiS/NiS_2	416(100)	156.5	2.4	Carbon cloth	3
$FeNi_2S_4$	273(10)	66	0.75	Nickel foam	4
MoS_2/NiS_2	278(10)	91.7	NA	Carbon cloth	5
NiS_2	375(10)	138	-	Carbon cloth	6
N-CNTs@NiS_2/Fe_7S_8	330(50)	51.49	0.22	GC	7
(Ni,Fe)S_2/NiFe(3:1)-CNFs	263(10)	52	1.63	GC	8

N-doped carbon/NiS_2	264(10)	51.3	2.4	Carbon cloth	9
FeS_2/NiS_2	280(50)	33	0.48	Carbon paper	10

References

1 J Tian, X. Xing, Y Sun, X. Zhang, Z Li, M Yang and G Zhang, Strongly coupled Fe-doped NiS_2/MoS_2 composite for high-efficiency water splitting, *Chem. Commun*., 2022, **58**, 557-560.

2 X Huang, L Yu, X Wang and L Feng, Insights into Fe-doping effect induced heterostructure formation for oxygen evolution reaction, *Chem. Commun.*, 2023, **59**, 12294-12297.

3 Q. Li, D Wang, C. Han, X. Ma, Q Lu, Z Xing and X Yang, Construction of amorphous interface in an interwoven NiS/NiS_2 structure for enhanced overall water splitting, *J. Mater. Chem. A*, 2018, **6**, 8233-8237.

4 H. Wang, J Tang, Y Li, H. Chu, Y Ge, R Baines, P. Dong, P Ajayan, J Shen and M Ye, Template-free solvothermal preparation of ternary $FeNi_2S_4$ hollow balloons as RuO_2-like efficient electrocatalysts for the oxygen evolution reaction with superior stability, *J. Mater. Chem. A*, 2018, **6**, 19417-19424.

5 J Lin, P Wang, H Wang, C. Li, X Si, J Qi, J. Cao, Z Zhong, W Fei and J Feng, Defect-rich heterogeneous MoS_2/NiS_2 nanosheets electrocatalysts for efficient overall water splitting, *Adv. Sci.*, 2019, **6**, 1900246.

6 X Zheng, X Han, Y Zhang, J Wang, C. Zhong, Y Deng and W Hu, Controllable synthesis of nickel sulfide nanocatalysts and their phase-dependent performance for overall water splitting, *Nanoscale*, 2019, **11**, 5646-5654.

7 J Wang, W Liu, X Li, T yang and Z Liu, Strong hydrophilicity NiS_2/Fe_7S_8 heterojunctions encapsulated in N-doped carbon nanotubes for enhanced oxygen evolution reaction, *Chem. Commun*., 2020, **56**, 1489-1492.

8 M Zhong, N. Song, C Li, C. Wang, W. Chen and X Lu, Controllable growth of Fe-doped NiS_2 on NiFe-carbon nanofibers for boosting oxygen evolution reaction, *J. Colloid Interface Sci.*, 2022, **614**, 556-565.

9 D Zhang, H Mou, L. Chen, G. Xing, D Wang and C Song, Surface/interface engineering N-doped carbon/NiS_2 nanosheets for efficient electrocatalytic H_2O splitting, *Nanoscale*, 2020, **12**, 3370-3376.

10 L. Wu, J Li, C. Shi, Y Li, H Mi, L Deng, Q Zhang, C He and X Ren, Rational design of the FeS_2/NiS_2 heterojunction interface structure to enhance the oxygen electrocatalytic performance for zinc-air batteries, *J. Mater. Chem. A*, 2022, **10**, 16627-16638.